Spectroscopy and Relaxation Kinetics of Matrix-Isolated CH/D Radicals†

Amy Burroughs and Michael C. Heaven*

Department of Chemistry, Emory University, Atlanta, Georgia 30322

Received: December 13, 1999; In Final Form: January 21, 2000

The $A^2\Delta-X^2\Pi$ and $B^2\Sigma^- - X^2\Pi$ transitions of CH/D were examined for radicals trapped in Ar and Kr matrixes. Excitation spectra yield further evidence that CH/D(B) rotates in solid Ar and Kr. Vibrational relaxation of CH/D(B) is faster for the heavier isotope, indicating that vibration to rotation energy transfer is the dominant mechanism. The decay of CH(B), $v = 0$ is primarily radiative in both Ar and Kr, with small contributions from B → A nonradiative transfer. Fluorescence was not detected from CD(B), $v = 0$ as the B → A transfer process was much faster than radiative decay for this isotope. The proximity of the CD(B), $v = 0$ and (A), $v = 1$ levels is responsible for the accelerated transfer rate. Spectra for the $A-X$ transition of $CH-Ar_n$ clusters were recorded for comparison with the matrix data. Relative to free CH, the transition is blue-shifted in the cluster and red-shifted in an Ar matrix. This contrast suggests that the clusters consist of CH bound to the surface of Ar_n.

1. Introduction

Molecules trapped in cryogenic rare-gas matrixes provide model systems for examining the properties of solvated species. Quantitative models of solvated species can be constructed when the potential energy surfaces resulting from pairwise interactions and many-body forces are known. Spectroscopic studies of van der Waals clusters are a valuable source of information regarding such interactions.[1−5] Over the past few decades, studies of clusters have yielded valuable insights regarding the spectral shifts and relaxation dynamics of matrix-isolated molecules.[3,6−8] The majority of this work has focused on closed-shell molecules. To date, there have been relatively few attempts to correlate the properties of open-shell molecules in matrixes and clusters.[5,9,10] This is a topic of some chemical significance, however, as knowledge of the effects of solvation on radicals is needed to fully comprehend condensed-phase reaction dynamics. In recent years, we have used CN−Rg clusters and matrixes to examine the electronic relaxation dynamics of a solvated radical.[5,11−13] The dynamics for CN isolated in solid Ar were found to be dramatically different from the dynamics exhibited by large $CN-Ar_n$ clusters.[11] The origin of this effect was traced back to the fact that CN resides on the surface of the cluster.[13]

The present work represents the beginning of an effort to understand the properties of matrix-isolated CH radicals using potential energy surfaces and insights derived from studies of $CH-Ar_n$ clusters.[14−17] Here, we describe a reinvestigation of the electronic spectroscopy and relaxation dynamics of CH in Ar and Kr matrixes.

Electronic absorption and emission spectra for matrix-isolated CH were first reported by Keyser.[18] The radical was produced by X-ray irradiation of methane in solid Ar. Absorption spectra for the $A^2\Delta-X^2\Pi$, $B^2\Sigma^- - X$, and $C^2\Sigma^+ - X$ transitions were recorded following X-ray exposure. Emission spectra, recorded during irradiation, revealed emissions from the same three electronic band systems. Fine structure was observed in the bands, some of which was tentatively assigned to nearly free rotation of CH in the B and C states. X-ray irradiation of CH_4/Kr matrixes was much less effective in generating CH. For CH in Kr, Keyser[18] reported no emissions and only one absorption band, assigned to the C−X system.

Milligan and Jacox[19] observed CH/D absorption spectra during a study of the vacuum ultraviolet photolysis of methane in solid Ar. Transition energies for A−X, B−X, and C−X bands of CH and CD were reported. Bhatnagar et al.[20] used pulsed laser excitation to examine the relaxation dynamics of CH and CD in Ar matrixes. In this study, the radicals were generated by passing mixtures of Ar with methane or acetylene through a microwave discharge prior to deposition. Bhatnagar et al.[20] found that excitation of the B−X origin band produced emissions from both the B−X and A−X band systems. They considered the possibility that the A state was being populated by matrix-induced nonradiative transfer from the B state and searched for evidence of this process. Action spectra, recorded by scanning the excitation wavelength while monitoring the A−X emission, appeared to be structureless in the region of the B−X (0,0) band. From this observation, Bhatnagar et al.[20] concluded that the A state was being populated directly, even though the excitation energy was several thousand wavenumbers above the A−X origin band. Fluorescence decay lifetime measurements were used to examine vibrational relaxation in the B states of CH and CD. Vibrational relaxation was found to be faster for the lighter isotope. This trend was taken as evidence that vibration to rotation energy transfer was the dominant relaxation mechanism. Bhatnagar et al.[20] reported origin band positions for the A−X and B−X systems of CD that were coincident with the corresponding bands of CH. Their assignment of the CD origins was tentative, as CH was also present in their deuterated samples.

Magnetic circular dichroism (MCD) spectra for the A−X and B−X transitions of CH in solid Ar were obtained by Rose[21] and Langford and Williamson.[22] From these data, Rose[21] concluded that CH(X) was oriented in the matrix cage and that spin−orbit coupling was completely quenched by the interactions with the surrounding lattice. Following the work of Keyser,[18] Rose[21] assigned the structure in the absorption bands

† Part of the special issue "Marilyn Jacox Festschrift".

* Corresponding author.

10.1021/jp994401g CCC: $19.00
Published on Web 03/01/2000

to rotation of CH(A/B). Langford and Williamson[22] extended the analysis of the MCD data, using a crystal field model to describe the guest−host interactions. For CH(X) they found that the spin−orbit coupling was partially quenched and derived a combined spin−orbit plus crystal field splitting of 81 cm^{-1}.

Details of the pairwise interactions between CH and Ar have been deduced from studies of the CH−Ar van der Waals complex.[14−17] Partial quenching of the ground-state spin−orbit coupling is evident as the rotational energy level pattern is characteristic of a $^2A''$ state.[14,15] For CH(X)−Ar, both the spectroscopic data and the theoretical calculations are consistent with a T-shaped equilibrium structure.[14,16] The excited-state complexes CH(A/B)−Ar are less tightly bound and have linear, hydrogen-bonded equilibrium structures.[14,16,17] Hence, the B−X and A−X transitions are blue-shifted relative to the transitions of free CH (by 81 and 98 cm^{-1}, respectively), and the spectra show progressions in the van der Waals stretch and librational modes. The blue-shift of the complex transitions was somewhat surprising, given that the transitions red-shift in rare-gas solids.[18−20,22]

In the present study, we have recorded new data for CH and CD in rare-gas matrixes. Slow B → A population transfer was observed for CH in Ar and Kr. For CD, this process was found to be so rapid that fluorescence from B, $v = 0$ could not be detected. The dramatic difference in the B → A transfer rates for CH and CD can be understood in terms of a simple energy gap model. Action spectroscopy was used to observe the CD B−X (0,0) band in Ar and Kr. Analysis of the structure of this band yields further evidence that CH/D(B) can rotate in solid Ar and Kr. To obtain insights regarding the contrasting spectral shifts produced by the matrix and complex environments, we briefly examined the A−X transition of CH−Ar_n ($n \sim 10-50$) clusters. Increasing the size of the cluster did not reverse the sign of the spectral shift (such behavior has been observed for $C_6F_6^+$−Ar_n complexes[9]). The contrast between the matrix and the cluster shifts is interpreted in terms of morphology differences.

2. Experimental Section

The matrix isolation unit used for this work has been described previously.[23] CH was produced by dissociation of methane. Methane/Rg mixtures were prepared in a vacuum line and stored in a glass bulb prior to deposition. CH_4 (Specialty Gases Southeast, UHP), CD_4 (Icon Isotopes, 99%D), Ar (Specialty Gases Southeast, UHP), and Kr (Nova Gas Technologies, UHP) were used without further purification. A discharge flow system was used to generate CH/D radicals prior to deposition. A flow of pure Ar or Kr (≈2 Torr) was passed through a microwave discharge and expanded through a 2-mm orifice into the high-vacuum matrix isolation chamber. The orifice was positioned 5 cm from a copper mirror that was held at 10−15 K by a closed-cycle refrigerator. Discharge conditions were adjusted so that the region excited extended to the end of the discharge tube. A small flow of the CH_4/D_4:Rg mixture was added on the downstream side of the orifice. CH_4/D_4 was dissociated by Rg metastables and VUV radiation from the discharge. Flow rates were chosen to produce an initial methane: Rg dilution ratio of 1:800 for the combined flows. Mixtures were deposited at a rate of approximately 7 mmol/h for Ar mixtures and 3.5 mmol/h for Kr mixtures for total depositions of 12 mmol. To increase the concentration of trapped CH/D in the samples, matrixes were photolyzed by the 193-nm output from an ArF laser after deposition. Samples were held at temperatures between 10 and 15 K for all spectroscopic measurements. The effects of annealing were examined by warming the substrate to ∼20 K over a period of approximately 5 min and then immediately cooling it back down.

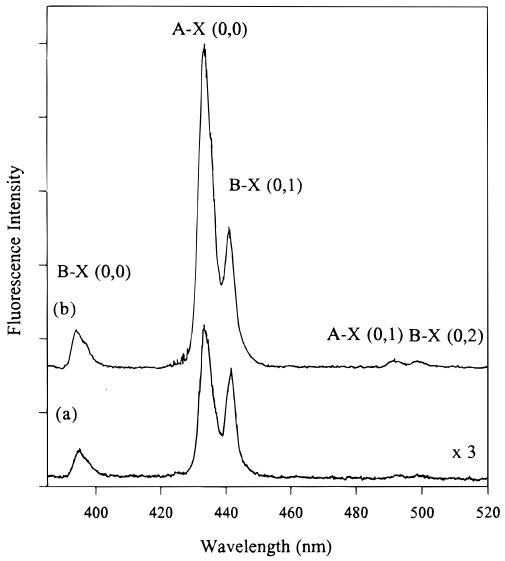

Figure 1. Emission spectra for CH isolated in solid Ar. The sample was excited by 389-nm light. Traces recorded (a) before and (b) after 10 min of photolysis with 193-nm radiation.

Species trapped in the matrixes were probed using laser-induced fluorescence techniques (LIF). Fluorescence was excited by either a pulsed tunable dye laser (0.3 cm^{-1} line width, Lambda Physik FL3002/EMG 101) or a pulsed discharge laser (Lumonics TE-860-4) with either ArF (193 nm) or N_2 (337 nm) as the gain medium. The wavelength output of the dye laser was calibrated by simultaneously recording Te_2 B−X spectra. Fluorescence from the matrix was collected by a collimating lens and focused through the entrance slits of a 0.64-m monochromator (ISA). In most experiments, long-pass filters were used to block laser scatter. Fluorescence was detected by a photomultiplier tube (RCA C31034). Signals were recorded using a digital oscilloscope (LeCroy ScopeStation 140) or boxcar integrator (SRS model 250) interfaced to a personal computer. A boxcar gate width of 0.2 μs was used for the recording of emission and excitation spectra. Fluorescence decay curves were recorded using the signal-averaging capabilities of the digital oscilloscope.

The free-jet expansion apparatus used to generate CH−Ar_n clusters has been described previously.[24] CH was generated by 248-nm photolysis of bromoform in the early stages of the expansion. The expansion was driven by a mixture of Ar (60%) and He (40%). Gas mixtures at source pressures in the range of 2.6−3.7 atm were expanded through a 0.8-mm orifice. CH−Ar_n clusters were detected via LIF of the A−X bands. The probe laser was positioned approximately 5 mm from the nozzle orifice.

3. Results

3.1. CH:Ar Matrixes. Figure 1 shows dispersed fluorescence spectra obtained by exciting the B−X (0,0) band at 389 nm. Emissions from B, $v = 0$ and A, $v = 0$ account for all of the features in these traces. The lower and upper traces were obtained before and after 193-nm photolysis, respectively. These spectra show that 193-nm photolysis increased the concentration of CH in the sample and increased the intensity of the A−X bands relative to B−X emission (note that the lower trace was multiplied by a factor of 3 to facilitate comparison). Photolysis periods ranging from 5 to 90 min were investigated. Irradiation

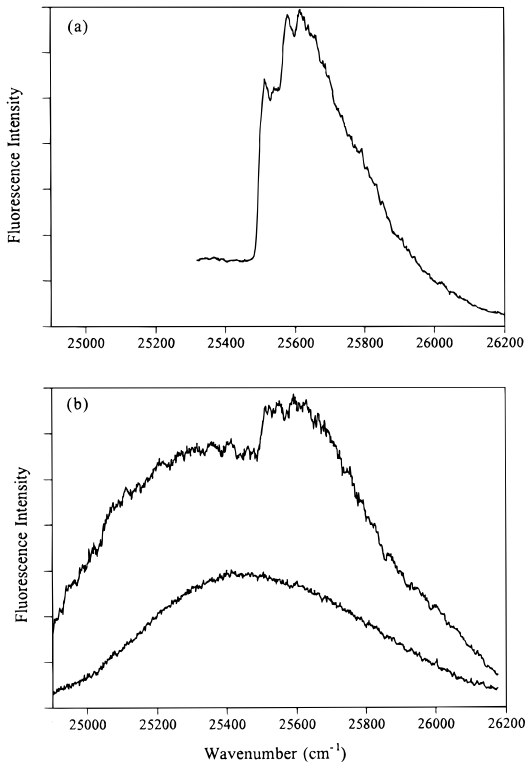

Figure 2. (a) CH B−X (0,0) excitation spectrum recorded from an Ar matrix after photolysis by 193-nm radiation. Fluorescence was detected on the B−X (0,1) band at 440 nm. This spectrum was not corrected for variations in the dye laser power. (b) Action spectrum for the B−X (0,0) band of CH in Ar. This trace was recorded by monitoring the A−X (0,0) band emission at 433 nm. The dye laser output power curve (lower trace) is shown for comparison.

for 5 min produced the same increase in fluorescence intensity as exposure for 90 min. To examine the possibility that photolysis generated CH by multiphoton dissociation of CH_4, Ar/CH_4 matrixes were prepared without running the microwave discharge. Extensive irradiation of these samples at 193 nm did not produce detectable amounts of CH.

Dispersed fluorescence spectra recorded at a higher instrumental resolution showed that the emission bands were relatively unstructured (the resolution was limited by phonon wing broadening). Our results for the emission band contours were essentially the same as those reported by Keyser[18] and Bhatnagar et al.[20]

Excitation spectra were obtained by tuning the dye laser through the B−X absorption features while monitoring a specific emission band. Figure 2a shows an excitation spectrum for the (0,0) band region obtained by monitoring the B−X (0,1) emission band at 440 nm. The structure in this spectrum was repeatable and had been noted previously.[18,21,22] The upper trace in Figure 2b shows a B−X excitation spectrum obtained by monitoring the A−X (0,0) band emission at 433 nm. Fluorescence from the A state was observed for excitation wavelengths in the range of 385−400 nm (the tuning range of the laser dye used). The dependence of the dye laser power on wavelength, monitored using a photodiode, is shown as the lower trace in Figure 2b. Comparing the excitation spectrum with the laser gain curve, it is evident that the spectrum contained only one element of structure, the intensity step at 392.1 nm that coincides with the B−X (0,0) feature. The spectra in Figure 2 were recorded after the samples had been photolyzed using 193-nm light. Similar results were obtained before photolysis, with lower signal-to-noise ratios.

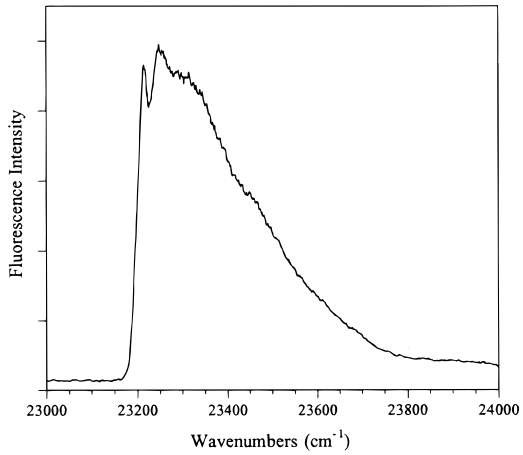

Figure 3. Excitation spectrum of the A−X (0,0) band for CH in Ar. This trace was obtained by detecting A−X (0,1) emission at 491 nm. The sample had been photolyzed and annealed. The spectrum was not corrected for variations in the dye laser power.

Excitation and dispersed fluorescence spectra were recorded using direct excitation of the A−X transition. An excitation spectrum of the (0,0) band, recorded by monitoring the (0,1) band at 491 nm, is shown in Figure 3. This feature has the general appearance of a zero phonon line accompanied by a strong blue-shaded phonon wing. Dispersed fluorescence spectra taken with excitation of the zero phonon line exhibited just the A−X (0,0) and the (0,1) bands. Excitation of the phonon wing yielded the same A−X bands, identical in appearance to those observed by exciting the zero phonon line. However, two new emission bands at 447 and 473 nm were present for excitation wavelengths in the 420−424-nm range. These features do not correspond to any known transitions of CH, and we attribute them to an unidentified product of secondary reactions that occurred during deposition.

Dispersed fluorescence spectra were recorded with higher energy excitation. Emissions induced by 337-, 308-, and 193-nm excitation were examined. All three wavelengths correspond to excitation above the B state dissociation limit. The spectra were similar to those recorded with excitation near the B−X origin, with the following exceptions: First, the B−X (1,1) transition was observed. Second, as the excitation energy increased, the intensity of emission from the A state increased relative to the B−X bands. Finally, an emission peak centered at 379 nm was observed for 337-nm excitation. On the basis of the work of Brus and Bondybey,[25] the 379-nm peak was assigned to the NH $A^3\Pi \rightarrow X^3\Sigma^-$ (0,1) transition (Bhatnagar et al.[20] also observed NH in their CH/Ar matrixes).

Annealing the CH/Ar matrixes after photolysis induced further changes in the emission and excitation spectra. To illustrate the effect on the dispersed fluorescence spectrum, traces recorded before and after annealing are compared in Figure 4. The upper spectrum was taken following 193-nm photolysis, while the lower spectrum was taken after warming the same matrix to ∼20 K and then cooling it back down. The annealing process produced an overall decrease in intensity and a decrease in the intensity of the A state emission peaks relative to the B−X emission peaks. In essence, annealing reversed the effects of 193-nm photolysis.

Figure 5a shows a B−X excitation spectrum taken after annealing. As compared to the spectrum in Figure 2a, annealing produced a sharpening of the structured part of the band contour. An intensity shift from the phonon wing to the zero phonon line was observed in both B−X and A−X excitation spectra after annealing.

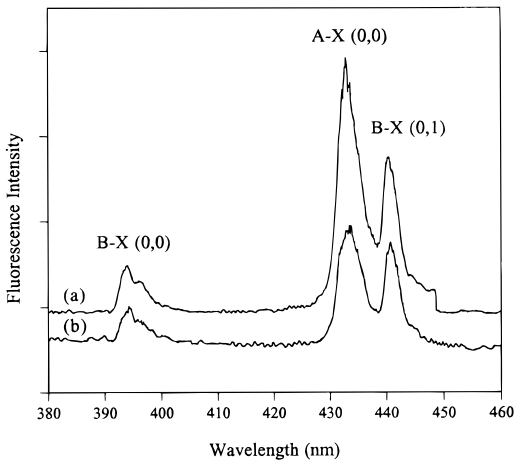

Figure 4. Emission spectra for CH in solid Ar. This sample was photolyzed at 193 nm. Traces were then recorded using 389-nm excitation (a) before and (b) after annealing the matrix.

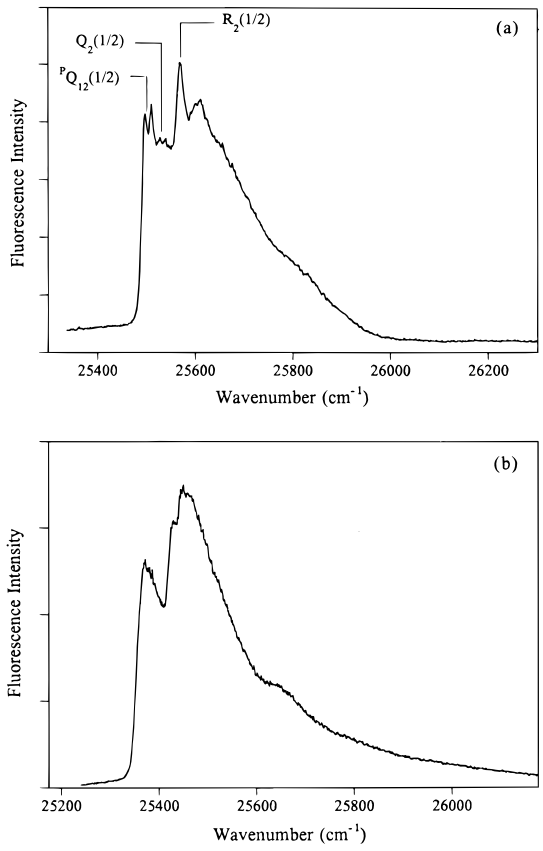

Figure 5. (a) Excitation spectrum for the CH B−X (0,0) band in solid Ar. This trace was taken after annealing with detection of the B−X (0,1) emission. Assignments for CH rotational transitions are indicated. (b) Excitation spectrum for the CH B−X (0,0) band in solid Kr. The matrix had not been annealed.

Red-shading of the dispersed fluorescence bands and blue-shading of the excitation features were evident in both the B−X and the A−X spectra. This characteristic, which was also noted by Keyser,[18] shows that much of the shading is due to phonon excitation. For bands that could be seen in both excitation and emission, the transition energies for the blue edges of the excitation bands coincided with the red edges of the emission features. Hence, the band edges correspond to zero phonon transition energies. Excitation spectra were used to determine the zero phonon transition energies, which are collected in Table 1. These data were taken from the excitation spectra as they were recorded at the highest resolution (0.3 cm^{-1}) and calibrated against an accurate standard. As can be seen in Figures 2, 3, and 5, the zero phonon features were not particularly sharp, so their positions were determined with an uncertainty of ±8 cm^{-1}.

TABLE 1: Transition Energies and Matrix Shifts for CH/D in Solid Ar and Kr[a]

	gas phase	Ar matrix		Kr matrix	
	ν	ν	Δ	ν	Δ
CH A−X	23247.5[b]	23217	31	23114	134
CD A−X	23235.3[c]	23223	12	23111	124
CH B−X	25698.2[b]	25501	197	25369	329
CD B−X	25793.1[c]	25615	178	25478	315

[a] Positions and shifts are in cm^{-1}. Error limits are ±8 cm^{-1} for matrix data. [b] Bernath, P. F.; Brazier, C. R.; Olsen, T.; Hailey, R.; Fernando, W. T. M. L.; Woods, C.; Hardwick, J. L. *J. Mol. Spec.* **1991**, *147*, 16. [c] Gero, L. Z. *Phys*. **1942**, *118*, 27.

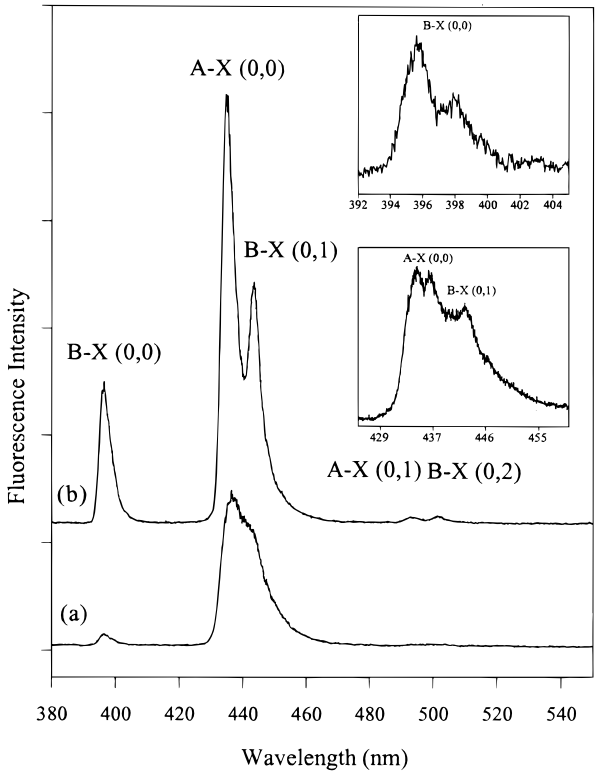

Figure 6. Emission spectra for CH isolated in solid Kr with 388-nm excitation (a) before and (b) after 193-nm photolysis. The insets show higher resolution emission spectra for the A−X (0,0) and B−X (0,0) transitions recorded prior to photolysis.

3.2. CH:Kr Matrixes. LIF and dispersed fluorescence spectra for CH/Kr matrixes were red-shifted relative to the corresponding features for CH in solid Ar. In most other respects, the properties of CH and other discharge products trapped in solid Kr and Ar were very similar (at least for the measurements carried out in this study). With excitation of the B−X (0,0) band, both B−X and A−X emissions were observed. As shown in Figure 6, photolysis of the Kr matrixes produced an increase in the CH concentration and a greater relative increase of the A−X band intensities. The inserts in Figure 6 show the emission features at a higher resolution. The B−X and A−X (0,0) bands were split into two peaks in Kr, which was not seen in Ar. The effect of photolysis on the relative intensities of the A−X peaks can be seen in Figure 7. The higher energy peak increased in intensity, while there was little change in the intensity of the lower energy peak (note that photolysis of the Kr matrixes also caused a sharpening of the emission features). Similarly, spectra

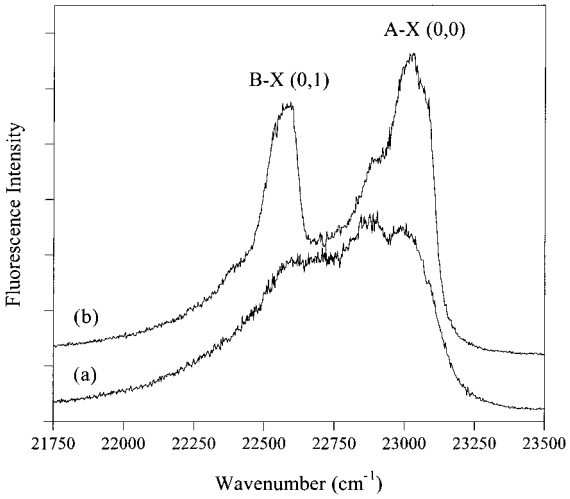

Figure 7. Emission spectra for the A−X (0,0) and B−X (0,1) transitions of CH in Kr (388-nm excitation) recorded (a) before and (b) after 30 min of 193-nm photolysis.

for the B−X (0,0) emission show that the higher energy peak gains intensity on photolysis. The fact that the relative intensities of the peaks can be modified by photolysis suggest that the splitting is a site effect.

An excitation spectrum for the B−X (0,0) band of CH in Kr is shown in Figure 5b, where the contour may be compared with a corresponding spectrum taken in Ar. The spectrum from the Kr matrix is red-shifted and less well resolved (the transition energy for the zero phonon line is given in Table 1). However, it is clear that the bands recorded in Kr and Ar have the same pattern of low-frequency structure. Note that the spacings between the resolved peaks are much smaller than the site splittings described above (the excitation spectrum in Kr was recorded with detection of the B−X (0,1) band at 443 nm). An excitation spectrum for the region around the B−X (0,0) band was also recorded using detection of the A−X (0,0) emission. Excitation throughout the 380−400 nm yielded A state emission, but the B−X (0,0) band contour was observed superimposed on the structureless background. The result was analogous to the Ar matrix spectrum shown in Figure 2b, but in Kr, the B−X feature was more intense relative to the unstructured component.

An excitation spectrum for the A−X (0,0) band in Kr, recorded with detection of the (0,1) emission, was entirely similar to the Ar result shown in Figure 3. The zero phonon transition energy is given in Table 1. A dispersed fluorescence spectrum was recorded using exciation of the phonon wing at 430 nm. The A−X emission bands observed by this means did not show the doublet splitting described above. Instead, just the higher energy member of the doublet was present. These data were recorded after 193-nm photolysis of the sample, which favors the site associated with the higher energy emission band.

Resolved fluorescence spectra were also examined for higher energy excitation wavelengths (337 and 193 nm). Emissions from both the B−X and the A−X bands were seen. Increasing the exciation energy increased the intensity of the A−X system relative to the B−X bands and favored emission from the higher energy members of the doublets. Annealing of the Kr matrixes reversed the effects of 193 nm photolysis. The relative intensities of the emission doublets and A−X versus B−X bands returned to their prephotolysis ratios.

3.3. CD:Ar and CD:Kr Matrixes. As with the CH matrixes, CD concentrations could be increased by exposing the samples to 193-nm light after deposition. Consequently, most spectra

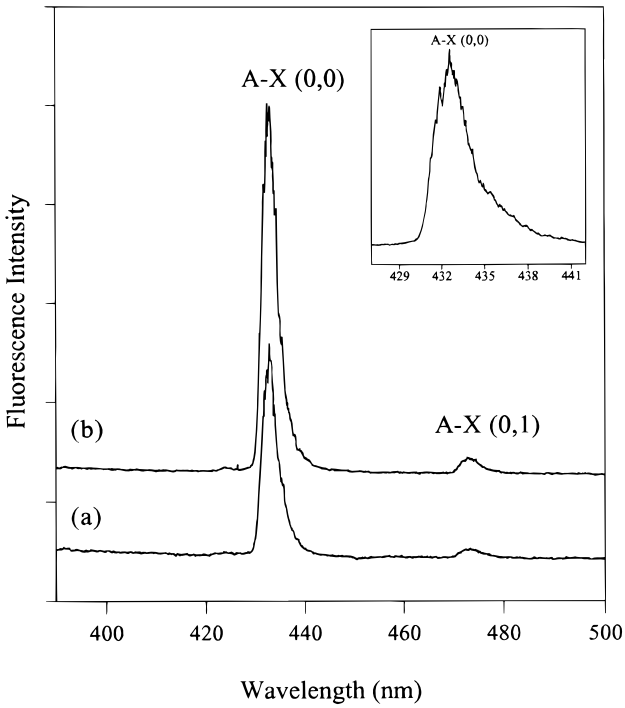

Figure 8. Emission spectra for CD isolated in solid Ar (a) before and (b) after 10 min of 193-nm photolysis. The inset shows the A−X (0,0) band at higher resolution. These traces were recorded using excitation of the B−X (0,0) band at 385 nm.

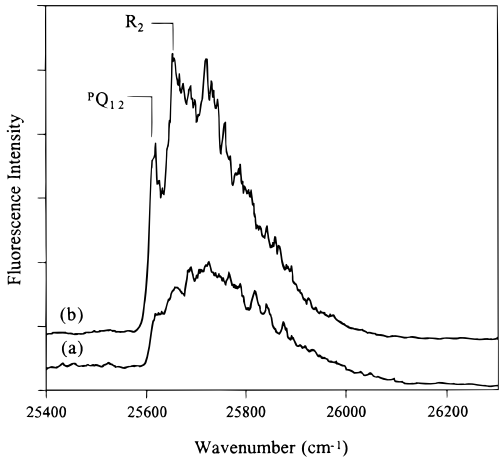

Figure 9. Action spectra for the CD B−X (0,0) band in Ar. These traces were obtained by monitoring the A−X (0,0) transition. (a) Recorded after 193-nm photolysis and (b) after annealing to 20 K. These spectra were not corrected for the dye laser gain curve.

were recorded after photolysis. Excitation of the B−X (0,0) band of CD in Ar resulted in vibrationally relaxed emission from the A state, as seen in Figure 8. The inset in this figure shows the (0,0) emission recorded with better resolution. The contour shows a zero phonon line with a strong phonon wing. Note that the B−X (0,0) and (0,1) bands, which would appear at 390 and 424 nm, are not present in Figure 8. In contrast to the behavior of CH in Ar, fluorescence from CD(B), $v = 0$ could not be detected. Analogous results were obtained for CD in Kr, a slight difference being that the A−X (0,0) zero phonon line was not as well-resolved in the heavier host.

Excitation (action) spectra for the CD B−X (0,0) band were obtained by detecting A−X fluorescence. The result of this measurement for CD/Ar is shown in Figure 9. Evidently, B → A transfer was much more rapid than B → X emission for the $v = 0$ level. As a consequence, the B−X feature is much

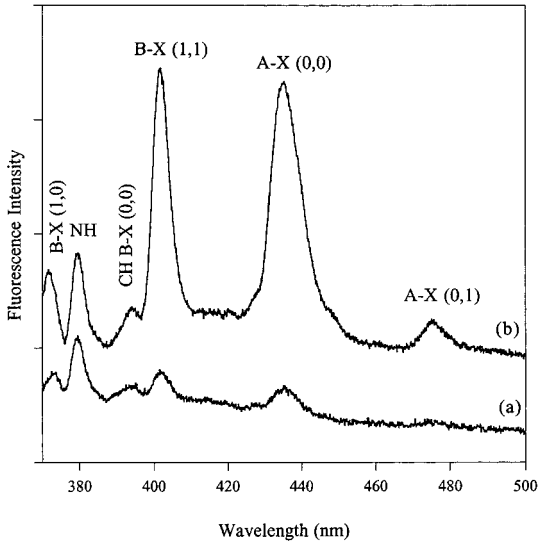

Figure 10. Emission spectrum for CD isolated in solid Ar with 337-nm excitation (a) before and (b) after 193-nm photolysis.

stronger than the broad, off-resonance background excitation. However, the latter was clearly present for CD. Low-frequency structure is apparent in Figure 9 and the corresponding spectrum recorded in Kr. The spacings between the resolved peaks were very similar for CD in Ar and Kr but smaller than the spacings in the B−X contours for CH in Ar or Kr. Figure 9 also shows that annealing the CD/Ar matrix sharpened the structure in the excitation band. The energies of the CD B−X (0,0) band zero phonon transitions in Ar and Kr are listed in Table 1.

Higher energy excitation (337 nm) was investigated to see if emission could be detected from vibrationally excited levels of CD(B). The resulting emission spectrum (Figure 10) exhibited the B−X (1,0) and (1,1) bands, along with emissions from A, $v = 0$.

Excitation of the A−X origin band yielded emission from the A, $v = 0$ level. Spectra taken from Ar and Kr matrixes were very similar in appearance to the CH A−X band shown in Figure 3. The zero phonon lines for CD were essentially unshifted from positions of the CH/Ar and CH/Kr A−X bands (cf. Table 1).

3.4. Fluorescence Decay Lifetimes. Fluorescence decay curves were recorded for all the CH/D transitions observed in emission. The majority of the decay curves (>90%) were clearly double exponential in character. There was a fast decaying component with a lifetime of <15 ns followed by a slower decaying component on the order of hundreds of nanoseconds. The fast component was attributed to laser scatter not blocked by the long-pass filter and filter fluorescence. The featureless excitation spectrum of this signal did not correlate with the CH/D absorption bands, and the temporal characteristics of the fast component were independent of excitation wavelength. The long-lived decay was only present when CH/D absorption bands were excited. Fluorescence decay curves for CH/D were fit using a double exponential function. Pretrigger recording was used to acquire the temporal waveforms, and the signal level prior to laser pulse was used to determine the baseline.

Fluorescence decay curves for CH(A), $v = 0$ and CH(B), $v = 0$ were recorded using excitation of different features within the absorption contours. For the B state, excitation of the zero phonon line, the low-frequency structure and the phonon wing yielded identical fluorescence decay lifetimes. Similarly, decay curves obtained by exciting the zero phonon line and phonon wing of the A−X (0,0) band gave the same characteristic lifetime for the A state. Lifetimes were also independent of the regions within the emission bands detected, including the double peaks of the A−X (0,0) and B−X (0,0) transitions for CH in Kr. Matrix manipulations such as 193-nm photolysis and annealing did not influence the observed decay curves.

TABLE 2: CH/D Lifetimes (ns)

assignment	gas phase[32,33]	previous work (Ar)[1]	τ (Ar)[a]	τ (Kr)[a]
CH A−X (0,0)	535	372 ± 7	289 ± 18	259 ± 4
			[532 ± 36]	[556 ± 8]
CH B−X (0,0)	328	233 ± 16	193 ± 7	172 ± 21
			[355 ± 14]	[369 ± 42]
CH B−X (1,0)	446	106 ± 3	161 ± 18	149 ± 35
			[297 ± 36]	[320 ± 70]
CD A−X (0,0)		306 ± 65	305 ± 15	274 ± 28
			[562 ± 30]	[588 ± 56]
CD B−X (1,0)	370	165 ± 30	258 ± 30	228 ± 25
			[475 ± 55]	[490 ± 54]

[a] Gas-phase lifetimes calculated from the matrix data using eq 1 are given in brackets.

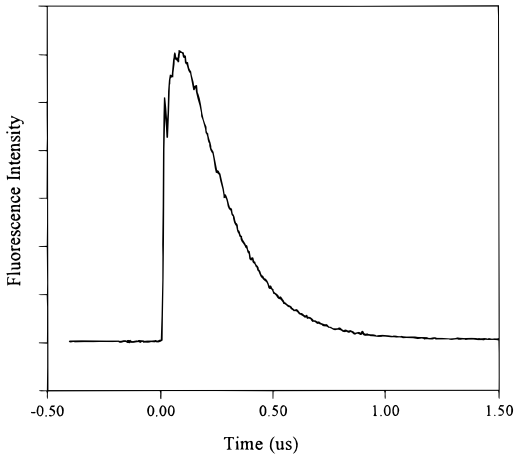

Figure 11. Time-resolved fluorescence for the B−X emission of CH in solid Ar. This trace was taken using 337-nm excitation and detection of the B−X (0,0) band.

Fluorescence decay lifetimes for CH/D are given in Table 2. The data correspond to direct excitation of the A and B, $v = 0$ levels. Emission from B, $v = 1$ was excited using 337-nm excitation. When excited by 337-nm light, emission from B, $v = 1$ was reasonably well represented by a single-exponential decay (ignoring the initial fast spike). However, as Figure 11 illustrates, emission from B, $v = 0$ clearly exhibited a finite rise time when 337-nm excitation was used.

For comparison, the lifetimes for CH and CD in Ar reported by Bhatnagar et al.[20] are also given in Table 2. Our results are in reasonable agreement with the earlier study, although the differences are outside the error limits.

3.5. CH−Ar$_n$ Clusters. LIF spectra for the A−X transition CH−Ar$_n$ clusters were recorded using source pressures in the range of 2−3.6 atm. Figure 12 shows spectra recorded using source pressures of 3 and 3.6 atm. From scaling relationships,[26] we estimate that the average number of Ar atoms in the clusters formed using the higher pressure expansion was around 50. The cluster spectrum consisted of two broad absorption peaks that extend a few thousand wavenumbers to the blue of the CH A−X origin. The peaks were separated by approximately 570 cm^{-1}. Their relative intensities were dependent on the source pressure, with the higher energy peak favored by increasing pressure. A search was made for cluster features on the low-frequency side of the CH A−X origin, but no additional bands were observed.

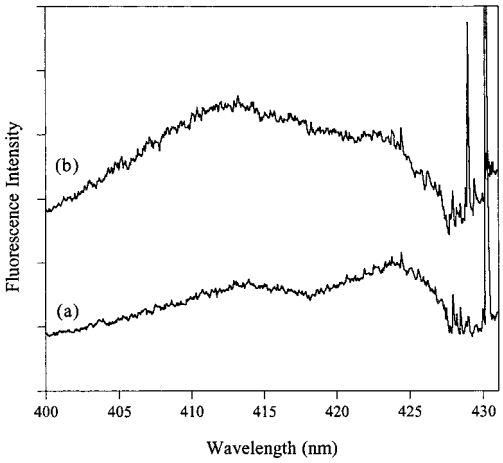

Figure 12. LIF spectra for CH−Ar$_n$ clusters with (a) 3 and (b) 3.6 atm source pressure. Fluorescence at 430 nm was monitored.

4. Discussion

4.1. Matrix Shifts. The transition energies for CH listed in Table 1 are in good agreement with previous measurements.[18−22] Data for CD in Kr have not been presented before, and the earlier report of emission from CD(B), $v = 0$ in Ar was incorrectly assigned[20] (CH emission was observed). As can be seen in Table 1, all of the transitions were red-shifted from the gas-phase values. The relative shifts were all less than 1.3%, and the direction and magnitudes of the shifts are typical for rare-gas solids. There are two points of interest here. First, the Kr shifts are appreciably greater than the Ar shifts, and they are not linearly dependent on the dielectric correction factor[27] $[(\epsilon - 1)/(2\epsilon + 1)]$. Second, shifts for the B−X transitions are greater than those for the A−X transitions. This is unexpected as the transitions occur in a similar energy range, and both excited states are derived from the same electronic configuration ($2p\sigma 2p\pi^2$). Furthermore, spectra for the CH−Ar binary complex[14,17] and ab initio calculations for CH(A)−Ar[28] and CH(B)−Ar[16] indicate that the pairwise interactions for the two excited states are of similar strength. At present we do not know the reason for the difference in matrix shifts for CH/D A and B. Vibrational intervals for the CH/D B and A states differed from the gas-phase values by less than 0.5%, indicating that the matrix had very little influence on the CH/D potential curves near the minima.

Langford and Williamson[22] predicted that a combination of crystal field and spin−orbit coupling terms should split the orbitally degenerate components of CH($X^2\Pi$) by 81 cm^{-1}. This splitting could not be observed in our emission spectra, but this was not necessarily in disagreement with the crystal field model. Phonon broadening of emission features exceeded 80 cm^{-1} and may well have obscured the structure.

4.2. Photolysis, Annealing, and Site Splittings. Irradiation of the matrixes at 193 nm resulted in an increase of the CH or the CD concentration. It was demonstrated that CH_4 was not the photolytic precursor to CH. The discharge method used to prepare the matrixes results in the trapping of CH_3 and CH_2, which are more promising precursors. Single photon excitation at 193 nm does not provide enough energy to produce CH from CH_3, but it is sufficient to dissociate CH_2. The process CH_2 + 193 nm → CH(X) + H has been characterized in the gas phase,[29] and it is the most probable source of photogenerated CH (or CD) in the present matrix studies.

Aspects of the photolysis and annealing behavior suggest that the photofragments (assumed to be CH and H to facilitate description) remain in fairly close proximity in the matrix. After photolysis, the emission from CH(A) was enhanced relative to the B−X system for excitation above B, $v = 0$. Annealing of the samples reduced the CH (or CD) concentration and returned the A−X versus B−X intensity ratio to the prephotolysis value. These observations can be rationalized by assuming that the photoproduct CH is weakly perturbed by a nearby H atom and that this perturbation facilitates nonradiative B → A transfer. In Ar matrixes, this perturbation was not large enough to produce measurable shifts of the band positions or increases in the fluorescence decay rates. On annealing, the H atoms diffuse back and recombine with the CH radicals, reversing the effects of photolysis.

The photolysis and annealing behavior of CH in solid Kr was used to show that doublet splittings in the emission spectra were due to site effects. The relative intensities of the doublet peaks were changed by photolysis, but their positions were unaffected. It seems that the higher energy site was preferentially created by photolysis.

4.3. Excitation Band Structures. Structure in the B−X (0,0) excitation (absorption) band of CH in Ar was observed in several previous studies. Keyser[18] recognized that the interval between the two strongest peaks was close to the spacing between the $R_2(1/2)$ and $^PQ_{12}(1/2)$ rotational lines of free CH. On this basis, the structure was tentatively assigned to rotation of CH within the matrix cage. Keyser[18] expressed some reservations in making this assignment as the $Q_2(1/2)$ line, which appears prominently between the $R_2(1/2)$ and the $^PQ_{12}(1/2)$ lines in the gas-phase spectrum, was not readily identifiable in the matrix spectrum. Subsequent investigators adopted the tentative assignment of the matrix spectrum. Rose[21] attributed the weak feature between $R_2(1/2)$ and $^PQ_{12}(1/2)$ peaks to the $Q_2(1/2)$ transition without commenting on the low relative intensity.

The results obtained in this study support assignment of the structure to CH/D(B) rotational motion. In Figure 5, excitation spectra for CH in Ar and Kr matrixes may be compared. Here, it can be seen that the separation between the two strongest features is almost unchanged in going from Ar to Kr. It is unlikely that the contours in the two hosts would be so similar if the structure arose from site splittings or vibrations of CH within the cage. The CD B−X band contours recorded in Ar and Kr are also similar to one another, but they are obviously different from the CH contours (compare Figures 5a and 9). Deuteration reduced the intervals between the peaks, as would be expected for structure associated with rotational motion.

Spectroscopic data for the CH−Ne van der Waals complex[30] provide insights regarding the weakness of the $Q_2(1/2)$ transition in solid Ar and Kr. Analysis of the B−X bands of the complex showed that rotation of CH(B) was only weakly hindered by the interaction with the Ne atom and that the total parity of the diatom was well defined within the complex.[30] Transitions from the ground-state zero point level (diatomic $j = 1/2$, + parity) accessed levels associated with the $R_2(1/2)$ and the $^PQ_{12}(1/2)$ lines of the diatom. The upper levels of these transitions correlate with Ne + CH(B), $n = 0$ and 2 levels, where n is the Hund's case b rotational quantum number for the diatom. Both levels are of − diatomic parity, in accordance with the usual − ↔ + dipole selection rule. Transitions of the complex associated with the $Q_2(1/2)$ line originate from the diatomic $j = 1/2$, − parity level and terminate on $n = 1$, + parity states. While the $j = 1/2$, ± levels are almost degenerate in free CH(X), the interaction with Ne separates them by 5 cm^{-1}. Hence, the $Q_2(1/2)$ transitions of the complex originate from an excited level of the ground state (see Figure 6 of ref 30). Note that

transitions from the zero point to $n = 1$, + levels are parity forbidden in as far as the diatomic parity is conserved in the complex. These transitions were too weak to be detected in the studies of CH−Ne carried out to date.

If CH is trapped in a high-symmetry lattice site, the diatomic parity will be conserved. The crystal field parameters reported by Langford and Williamson[22] predict that the ± parity components of the Π state will be widely split by the interaction with the host. In this situation, the $Q_2(1/2)$ line would be red-shifted from the position expected on the basis of the gas-phase spectrum and extremely weak due to the small thermal population of the lower level. The fact that spectrum of matrix-isolated CH does show a feature at the expected $Q_2(1/2)$ position suggests that some fraction of the CH radicals are trapped in sites where the symmetry is low enough to cause partial breakdown of the diatomic parity. This mixes diatomic − parity character into the ground-state zero point and B state $n = 1$ levels and thereby permits transitions between them.

The first two peaks in the B−X (0,0) band for CD in Ar (Figure 9) are separated by 35 cm^{-1}, which is consistent with assignment to the $R_2(1/2)$ and the $^PQ_{12}(1/2)$ lines. After the annealing, the contour also exhibits a third peak 95 cm^{-1} above the $^PQ_{12}(1/2)$ line. This interval is consistent with the CD(B), $n = 0-3$ rotational spacing. Assignment of the third peak to the B, $n = 3$ ($j = 5/2, 7/2$) → X, $n = 1$ ($j = 1/2$) transition implies that the $\Delta j = 0, \pm 1$ selection rule has been relaxed. The interaction with the matrix can mix states that differ in j, which would account for the breakdown of the selection rule. Furthermore, this mixing will be greater for CD than CH (which does not show an obvious third peak) as the rotational levels of the former are more closely spaced. There are, however, problems with assigning the third CD peak to the B, $n = 3 \rightarrow$ X, $n = 1$ transition. The implication is that the B, $n = 3$ level (and/or the X, $n = 1$ level) has acquired enough − parity character to produce a relatively strong transition. This level of parity mixing would also result in a strong $Q_2(1/2)$ feature, while the spectrum exhibits a rather weak absorption at the $Q_2(1/2)$ position. Assignment of the third peak to the CD(B), $n = 4$ level avoids the implication that the diatomic parity is compromised, but the position of the peak would then indicate that the rotational motion of CD(B) is significantly hindered by the host lattice. It seems probable that the third peak is associated with rotational motion of CD, but we cannot make a definite assignment for this feature using the available data.

The structure of the A−X (0,0) band contours is simpler than the B−X bands. However, the fact that only one sharp feature is seen does not imply that CH(A) is unable to rotate in solid Ar or Kr. Gas-phase rotational selection rules allow only one transition [$R_2(1/2)$] from the X, $j = 1/2$ level. For matrix-isolated CD, the selection rules may be relaxed, but structure associated with transitions to higher energy rotational levels cannot be readily discerned in the band contour. If such features are present, they have been masked by phonon broadening.

4.4. Relaxation Kinetics. Radiative lifetimes for excited states are shortened when molecules are isolated in rare-gas solids. The approximate expression[31]

$$\tau_{gas} = \tau_{matrix}\frac{n(n^2+2)^2}{9} \quad (1)$$

has been used frequently to relate gas-phase lifetimes (τ_{gas}) and matrix lifetimes (τ_{matrix}) via the refractive index of the host (n). In Table 2, gas-phase lifetimes for the A and B states of CH/D[32,33] are compared with lifetimes calculated using eq 1. For the CH, $v = 0$ levels, the calculated lifetimes are in good agreement with the gas-phase values, which indicates that these levels relax primarily by radiative decay.

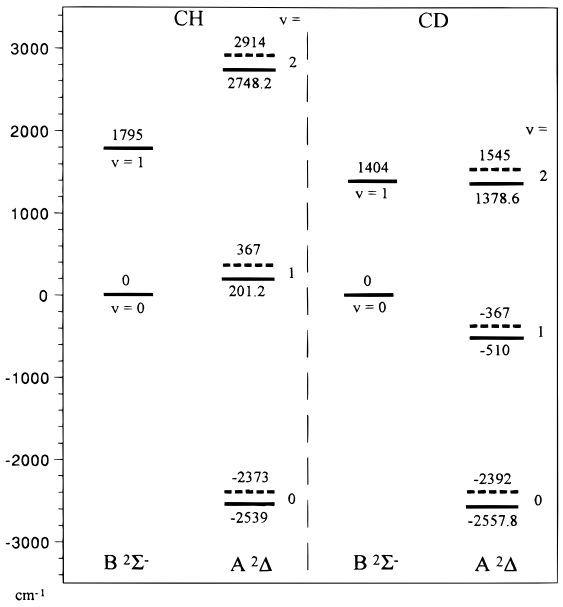

Figure 13. Energy level diagram showing the relative positions of A and B state vibrational levels. The energy scales are relative to the B, $v = 0$ levels of CH or CD. The energies of the levels in the gas phase and in an Ar matrix are indicated by solid and broken lines, respectively (the solid and broken lines are coincident for the B state levels).

Bhatnagar et al.[20] concluded that transfer from CH(B), $v = 0$ to the A state was negligibly slow in solid Ar. In the present study, we obtained an action spectrum (Figure 2b) which showed that a fraction of the B state population did transfer to the A state. Bhatnagar et al.[20] did not observe structure in their action spectrum because the output power of their dye laser was strongly dependent on wavelength in the region of the B−X (0,0) band (see Figure 3 of ref 20). The weakness of the B−X feature in Figure 2b indicates that B → A transfer is much slower than B−X radiative decay. This is consistent with the above discussion of the lifetime. The uncertainty in the B state lifetime is such that nonradiative decay channels with rates that are 10% or less of the radiative rate could not be discerned from the decay kinetics. Action spectra for CH in Kr show a somewhat stronger peak due to B → A transfer, but it is clear that B state nonradiative decay is also slow in this host.

On the basis of energy gap considerations, it is expected that B → A transfer for CH will be slow. Figure 13 shows the relative positions of the B and A state vibrational levels. Here, energies for gas-phase levels are given by solid lines, and the levels for CH in solid Ar are indicated by broken lines. For convenience, zero energy is defined by B, $v = 0$ for each set of levels. Transfer from CH(B), $v = 0$ to (A), $v = 0$ requires the dissipation of 2373 cm^{-1} of energy to an Ar lattice (2344 cm^{-1} in Kr), which is an improbable event. Transfer to A, $v = 1$ is not an open channel.

In section 3.3, we argued that B → A transfer was so rapid for CD that fluorescence from CD(B) could not be detected in solid Ar or Kr. The reason that transfer is so much faster for CD can be seen by inspection of the right-hand side of Figure 13, where relative positions of the A and B state levels of CD are shown. The energy gap for B, $v = 0$ to A, $v = 1$ is only 367 cm^{-1} in Ar (342 cm^{-1} in Kr). This small amount of energy is easily accommodated by the matrix. Figure 13 can also be used to explain why fluorescence is seen from CD(B), $v = 1$. In the matrix, this level is below A, $v = 2$ so the energetically

nearest level for B, $v = 1 \rightarrow$ A transfer has an unfavorably large energy gap (1771 cm^{-1}). Note that the different matrix shifts experienced by the A and B states plays an important role here. For CD in the gas phase, the A, $v = 2$ level lies just below B, $v = 1$. If this situation were preserved in the matrix, nonradiative relaxation of CD(B), $v = 1$ to (A), $v = 2$ would be fast. The matrix shifts render this channel inaccessible when CD is isolated in Ar or Kr.

From gas-phase measurements, it is known that CH(B), $v = 1$ has a longer radiative lifetime than B, $v = 0$. The fact that CH(B), $v = 1$ has a shorter fluorescence decay lifetime than B, $v = 0$ in Ar and Kr (see Table 2) shows that vibrational relaxation and/or B $\rightarrow$ A transfer contributes significantly to the $v = 1$ decay rate. Fluorescence decay lifetimes for CD(B), $v = 1$ are longer than those for CH, and surprisingly, they extrapolate to gas-phase lifetimes that exceed the radiative value. It is likely that the method used to obtain the $v = 1$ lifetimes was responsible for this apparent anomaly. Excitation of CH/D at 337 nm accesses states that lie above the $C(^3P) + H(^2S)$ dissociation asymptote. Vibrational levels of CH/D(B) are populated by relaxation and/or caged recombination. For CH(B), $v = 0$ the kinetics of populating the level are slow enough to produce a signal with a measurable rise time (as can be seen in Figure 11). For the $v = 1$ level, the transfer process was not so slow that the fluorescence signals exhibited obvious rise−fall characteristics, but convolution of the transfer and decay mechanisms may have lengthened the observed lifetimes relative to the values that would be observed for spontaneous decay alone. This could account for the long CD(B), $v = 1$ lifetimes and the fact that our lifetime for CH(B), $v = 1$ in Ar is greater than the value reported previously.

Bhatnagar et al.[20] noted that the lifetime of CD(B), $v = 1$ was longer than the CH(B), $v = 1$ lifetime in Ar matrixes. Our results for the lifetimes, although complicated by the excitation mechanism, show the same trend. Prior to the study of Bhatnagar et al., it had been noted that the rates for vibrational relaxation of OH(A)[34] and NH(A)[25] in Ne matrixes decreased when the molecules were deuterated. As the vibrational energy gaps are smaller for the heavier isotopes, this behavior is not easily explained in terms of direct energy transfer from the guest to lattice phonon modes. Instead, it has been assumed that relaxation proceeds by vibration−rotation energy transfer (V−R) within the diatom. This process is slower for the heavier isotope because near resonant transfer will involve a greater change in the angular momentum of the diatom. As rotation of CH/D(B) in Ar and Kr matrixes appears to be facile, it seems reasonable that V−R transfer is the primary nonradiative decay mechanism for CH/D(B), $v = 1$, as Bhatnagar et al.[20] concluded in their study.

4.5. Comparison of Cluster and Matrix Spectral Shifts. Spectra for the binary CH−Ar complex show A−X and B−X origin bands that are blue-shifted relative to free CH, while the transitions in rare-gas matrixes are red-shifted. Increasing the number of Ar atoms in the cluster produced a very broad, nearly structureless A−X feature that remained blue-shifted (Figure 12). We speculate that morphology differences are responsible for the opposite shifts for the clusters and matrixes. This behavior can be explained by assuming that the clusters consist of CH bound to the surface of an Ar_n cluster. CH(X) has one empty and one half-filled pπ orbital. Surface-bound clusters are particularly favorable for CH(X) as repulsive interactions can be minimized by pointing the empty pπ orbital toward the Ar_n cluster with the half-filled pπ orbital tangential to the surface. Electronic excitation to the A or B states promotes a second electron into the pπ orbitals. With more charge density moved off-axis a "hydrogen-bonded" geometry gives the lowest energy, and there is no longer a direction of approach that can take advantage of an empty orbital. Consequently, the excited states of CH do not bind as tightly to Ar_n as CH(X), and the transitions blue-shift.[14,16,17] When CH(X) is embedded in a rare-gas solid, repulsive interactions between the nearby lattice atoms and the half-filled pπ orbital will contribute to the ground-state energy. This destabilization of the ground state will certainly cause the transitions in the matrix to be red-shifted relative to the transitions for surface-bound clusters. The fact that the matrix transitions are red-shifted relative to free CH shows that there are additional (unidentified) factors influencing the relative stability of the ground and excited states in the matrix.

5. Summary

Laser excitation techniques have been used to examine the B−X and A−X transitions of CH/D isolated in Ar and Kr matrixes. Low-frequency structure was observed in the B−X (0,0) bands. This structure had been seen previously for CH in Ar. In the present work, new data for CH in Kr and for CD in Ar and Kr were recorded. The B−X band structure changed considerably on H/D isotopic substitution, while it was relatively insensitive to replacement of Ar by Kr. These observations support the notion, originally suggested by Keyser, that the low-frequency structure belongs to rotation of CH/D(B) within the matrix cage. Spectra for the A−X transition of CH/D did not show evidence of rotation in the cage, but it is likely that optical selection rules prevent the observation of rotational structure in this instance.

Relaxation of CH(B) was examined via action spectroscopy and time-resolved fluorescence decay measurements. The lifetime of B, $v = 0$ was consistent with predominantly radiative decay in Ar and Kr. However, action spectra show that B $\rightarrow$ A transfer makes a small contribution to the decay kinetics (<10%). Transfer was most efficient for CH that had been generated by in situ photolysis. This effect was attributed to perturbation of the photoproduct CH by nearby photofragments. Relaxation of CD(B), $v = 0$ via B $\rightarrow$ A transfer was found to be rapid in both Ar and Kr matrixes. Transfer was facilitated by the relatively small energy gap between B, $v = 0$ and A, $v = 1$ (a closed channel for CH).

In accordance with the work of Bhatnagar et al,[20] differences in the B, $v = 1$ lifetimes of CH and CD were ascribed to vibrational relaxation. The longer lifetime for CD(B), $v = 1$ was consistent with relaxation dominated by a vibration to rotation energy transfer mechanism.

Spectra for the A−X transition of CH−Ar_n clusters were examined. In contrast to the behavior of CH in solid Ar, the clusters exhibited a spectral blue-shift. We argue that this difference occurs because CH is bound to the outside of the Ar_n cluster, with the half-filled orbital tangential to the surface. In the matrix, repulsive interactions with the half-filled orbital increase the energy of the ground state relative to CH(A/B).

Acknowledgment. We are grateful to Mr. Anatoly Komissarov for his participation in the recording of the CH−Ar_n spectra and Professor Gene Trowbridge for assistance with computer interfacing the monochromator. This work was supported by the National Science Foundation under Grant CHE 9810106.

References and Notes

(1) Leutwyler, S.; Bosiger, J. *Chem. Rev.* **1990**, *90*, 489−507.

(2) Goyal, S.; Schutt, D. L.; Scoles, G. *Acc. Chem. Res.* **1993**, *26*, 123−130.
(3) Nesbitt, D. J. *Faraday Discuss.* **1994**, *97*, 1−17.
(4) Bacic, Z.; Miller, R. E. *J. Phys. Chem.* **1996**, *100*, 12945−12959.
(5) Heaven, M. C.; Chen, Y.; Lawrence, W. G. *Adv. Mol. Vib. Collision Dyn.* **1998**, *3*, 91−126.
(6) Anderson, D. T.; Davis, S.; Nesbitt, D. J. *J. Chem. Phys.* **1997**, *107*, 1115−1127.
(7) Hutson, J. M.; Liu, S.; Moskowitz, J. W.; Bacic, Z. *J. Chem. Phys.* **1999**, *111*, 8378−8383.
(8) Bacic, Z. *Theory At. Mol. Clusters* **1999**, 54−85.
(9) Kung, C. Y.; Miller, T. A. *J. Chem. Phys.* **1990**, *92*, 3297−3309.
(10) Heaven, M. C. *J. Phys. Chem.* **1993**, *97*, 8567−8577.
(11) Lin, H. S.; Erickson, M. G.; Lin, Y.; Basinger, W. H.; Lawrence, W. G.; Heaven, M. C. *Chem. Phys.* **1994**, *189*, 235−243.
(12) Lawrence, W. G.; Chen, Y.; Heaven, M. C. *J. Chem. Phys.* **1997**, *107*, 7163−7178.
(13) Chen, Y.; Heaven, M. C. *J. Chem. Phys.* **1998**, *109*, 2808−2813.
(14) Lemire, G. W.; McQuaid, M. J.; Kotlar, A. J.; Sausa, R. C. *J. Chem. Phys.* **1993**, *99*, 91−98.
(15) McQuaid, M. J.; Lemire, G. W.; Sausa, R. C. *Chem. Phys. Lett.* **1993**, *210*, 350−354.
(16) Alexander, M. H.; Gregurick, S.; Dagdigian, P. J.; Lemire, G. W.; McQuaid, M. J.; Sausa, R. C. *J. Chem. Phys.* **1994**, *101*, 4547−4560.
(17) Komissarov, A. V.; Kaledin, A. L.; Kerenskaia, G.; Heaven, M. C. Manuscript in preparation.
(18) Keyser, L. F. Ph.D. Dissertation, California Institute of Technology, 1965.
(19) Milligan, D. E.; Jacox, M. E. *J. Chem. Phys.* **1967**, *47*, 5146−5156.
(20) Bhatnagar, R.; Wilkerson, J. L.; Smith, G. R.; Guillory, W. A. *J. Mol. Spectrosc.* **1981**, *85*, 348−357.
(21) Rose, J. L. Ph.D. Dissertation, University of Virginia, 1987.
(22) Langford, V. S.; Williamson, B. E. *J. Phys. Chem. A* **1998**, *102*, 138−145.
(23) Nicolai, J. P.; Heaven, M. C. *J. Chem. Phys.* **1987**, *87*, 3304−3312.
(24) Heaven, M. C. *Annu. Rev. Phys. Chem.* **1992**, *43*, 283−310.
(25) Brus, L. E.; Bondybey, V. E. *J. Chem. Phys.* **1975**, *63*, 794−804.
(26) Hagena, O. F.; Obert, W. *J. Chem. Phys.* **1972**, *56*, 1793−1802.
(27) Bauer, E.; Magat, M. *J. Phys. Radium* **1938**, *9*, 319.
(28) Kaledin, A. L.; Heaven, M. C. Manuscript in preparation.
(29) Bohn, B.; Stuhl, F. *J. Chem. Phys.* **1995**, *102*, 8842−8845.
(30) Basinger, W. H.; Lawrence, W. G.; Heaven, M. C. *J. Chem. Phys.* **1995**, *103*, 7218−7227.
(31) Fulton, R. L. *J. Chem. Phys.* **1974**, *61*, 4141.
(32) Luque, J.; Crosley, D. R. *J. Chem. Phys.* **1996**, *104*, 2146−2155.
(33) Lugue, J.; Crosley, D. R. *J. Chem. Phys.* **1996**, *104*, 3907−3913.
(34) Brus, L. E.; Bondybey, V. E. *J. Chem. Phys.* **1975**, *63*, 786−793.